ELSEVIER

Measured optical constants of $Pd_{77.5}Cu_6Si_{16.5}$ bulk metallic glass

Lyndsey McMillon-Brown[a,b], Punnathat Bordeenithikasem[c,d], Ferra Pinnock[a], Jittisa Ketkaew[c],
Andrew C. Martin[e], Jan Schroers[c], André D. Taylor[a,f,*]

[a] Department of Chemical and Environmental Engineering, Yale University, New Haven, CT, 06511, USA
[b] Photovoltaic and Electrochemical Systems Branch, NASA Glenn Research Center, 21000 Brookpark Rd., Cleveland, OH, 44134, USA
[c] Department of Mechanical Engineering and Materials Science, Yale University, New Haven, CT, 06511, USA
[d] Engineering and Science Directorate, NASA Jet Propulsion Laboratory, California Institute of Technology, 4800 Oak Grove Dr., Pasadena, CA, 91109, USA
[e] J.A. Woollam, Inc., 645 M Street, Suite 102, Lincoln, NE, 68508, USA
[f] Department of Chemical and Biomolecular Engineering, New York University, 6 MetroTech Center, Brooklyn, NY, 11201, USA

ARTICLE INFO

Keywords:
Spectral ellipsometry
Optical properties
Refractive index
Bulk metallic glass

ABSTRACT

Optical constants of $Pd_{77.5}Cu_6Si_{16.5}$ alloy were determined experimentally using spectroscopic ellipsometry measurements on bulk specimens. Values of the complex refractive index of the glassy metallic alloys are compared to their crystalline counterparts and to pure crystalline Pd. The presence of Cu and Si increase the occurrence of defects in the crystal lattice resulting in reduced refractive index in the crystalline alloy when compared to pure crystalline Pd. Moreover, we show the conduction band energy of each specimen using Tauc's plot. The obtained complex refractive index across the spectrum (250–1500 nm) allows for accurate prediction of optical performance within the investigated spectral range providing optimal design for optical devices.

1. Introduction

Bulk metallic glasses (BMGs) represent a broad family of glasses comprised primarily of metallic elements [1]. Many BMGs have been developed since their discovery including Pd, Cu, Au, Ni, Ti, La, Zr, Fe, and Pt based alloys [2]. These metals form bulk amorphous phases when cast at cooling rates less than 100 K/s [3]. BMGs were originally considered for mechanical applications since they exhibit attractive structural properties that draw from both their glassy and metallic nature, including high strength [4,5], a large elastic strain limit [4,6], high hardness [6], and, in certain cases, substantial fracture toughness [4]. Previous studies, however have reported that BMGs can also be suitable for a wide range of applications. For example, our group demonstrated how nanoimprinted BMGs can be used for electrochemical catalyst applications [7–11]. BMG nanoparticles have been shown as a good candidates for lithium ion batteries [12], light harvesting [13], photovoltaics [14], biochemical [15], magneto-optical [16], organic synthesis [17] and biomedical systems [18,19]. Existing applications extend further, to include micro/nano electromechanical systems (MEMs/NEMs) devices [10,20,21]. The mechanical traits in addition to their high formability and facile processing capabilities, which allow for nano-scale features with angstrom-level smoothness [22], make BMGs an ideal candidate for applications such as photovoltaic cells or FETs

[2]. This rise in potential applications for BMGs increases the need to accurately characterize the materials optical properties. The optical properties of many BMGs are not well known and the suitability for use in optoelectronic devices is difficult to predict.

Here we provide optical properties of the Pd-Cu-Si alloy, necessary for implementation of BMGs into previously unexplored fields. Optoelectronic characterization of the BMG is particularly important for use in next-generation photovoltaics such as thin-film solar cell designs which often incorporate electrode patterning [23,24]. The designated $Pd_{77.5}Cu_6Si_{16.5}$ alloy composition is among the most highly studied BMGs, yet it has not been evaluated optically. Because this alloy also exhibits a high glass forming ability [25], it can be readily patterned and implemented into a wide range of device systems. $Pd_{77.5}Cu_6Si_{16.5}$ is among the few BMGs that can be fabricated with a critical size over 1 cm [26]. Determination of the optical constants, including the dielectric function and absorption coefficient, are necessary to predict the photo-active behavior of optically enhanced devices and prerequisite to determining the corresponding optical gap or generating a theoretical model. We note that a few other groups have investigated the optical [27,28] or electrical [29] properties of other Pd alloys. For example, a previous study conducted by Schlegel et al. investigated optical differences between amorphous $Pd_{81}Si_{19}$ and pure crystalline Pd [27]. They determined the optical constants of glassy

$Pd_{81}Si_{19}$ in a large energy range and showed that the results can be interpreted similarly to data on pure Pd as a superposition of intra- and interband transitions with quite similar energy ranges [27]. The $Pd_{81}Si_{19}$ alloy in this previous study was prepared via thin film sputtering and splat quenching which results in a different thermal history, and different resulting local atomic structure, than an alloy prepared by casting for this work. For our study, we aimed to investigate any observable changes between the crystalline and amorphous structures of a highly formable BMG. Hence, the differences in alloy preparation and composition make this work unique, and necessary for optical characterization of the $Pd_{77.5}Cu_6Si_{16.5}$ alloy. Thus, we report what we believe to be the first characterization of the constants for $Pd_{77.5}Cu_6Si_{16.5}$ alloy.

2. Methods

2.1. $Pd_{77.5}Cu_6Si_{16.5}$ sample preparation and characterization

The preparation of $Pd_{77.5}Cu_6Si_{16.5}$ metallic glass begins with high-purity (> 99.95%) constituent elements weighed according to their stoichiometric ratios and alloyed together to form a master alloy using an arc-melter. Next the master alloy is fluxed in anhydrous B_2O_3 at 1200 °C for 30 min to remove impurities [30,31]. The fluxed-alloy is then re-melted and cast into a 2 mm diameter rod using a quartz mold and subsequent water quenching to achieve amorphous $Pd_{77.5}Cu_6Si_{16.5}$ BMG. The as-cast rod was cut into cylindrical samples 2 mm tall and thermoplastically formed into disks [2]. We show a differential scanning calorimetry (DSC, PerkinElmer Diamond DSC) thermogram of the amorphous as-cast sample that the crystallization temperature of the $Pd_{77.5}Cu_6Si_{16.5}$ alloy is 422 °C at 20 K/min heating rate, verifying its amorphous structure and that the alloy fully crystallizes when heated about 600 °C. (Fig. 1(a)). To achieve the crystallized sample, an as-cast rod was heated to 700 °C, well-above the crystallization temperature, for over 30 min with anhydrous B_2O_3 as flux and under a vacuum of at least 10 mTorr to prevent oxidation. Then the furnace is switched off and the sample is allowed to cool in the furnace until 500 °C and then removed from the furnace to air cool.

Both the metallic glass and crystalline samples were ground in multiple steps using progressively finer abrasive SiC papers. Then, the samples were each polished using 1 μm polycrystalline diamond suspensions (Buehler MetaDi) until a final finish was achieved. After the samples were fabricated they were stored in nitrogen glove box and transported in a nitrogen environment, exposed to atmosphere and quickly characterized via spectral ellipsometry and X-ray diffraction (XRD) measurements. Efforts were made to prevent oxidation, even though the formation of Cu_2O is stochiometrically unfavorable for this alloy composition. We confirm using XRD the amorphous and crystalline structure for the bulk specimens ((Fig. 1(b and c) respectively). XRD measurements were made with a Rigaku SmartLab X-ray diffractometer with a Cu Kα radiation source.

2.2. Spectroscopic ellipsometry measurement

The refractive index of a material is an important parameter that must be identified to successfully implement novel materials into optical applications. We characterized the optical constants using variable angle spectroscopic ellipsometry (VASE). Ellipsometric measurements were carried out at room temperature with an angle of incidence (with respect to the normal of the sample) of 55° and 65°, using a dual rotating compensator spectroscopic ellipsometer (RC2 by J.A. Woollam), over the spectral range 250–1500 nm (0.82–5 eV). VASE measures changes in polarization of light as a function of incident angle and wavelength when light is reflected from or transmitted through a sample. The polarization change is described by an amplitude ratio, tan (Ψ), and phase difference, Δ, between light's electric field components which are oriented parallel (p) and perpendicular (s) relative to the
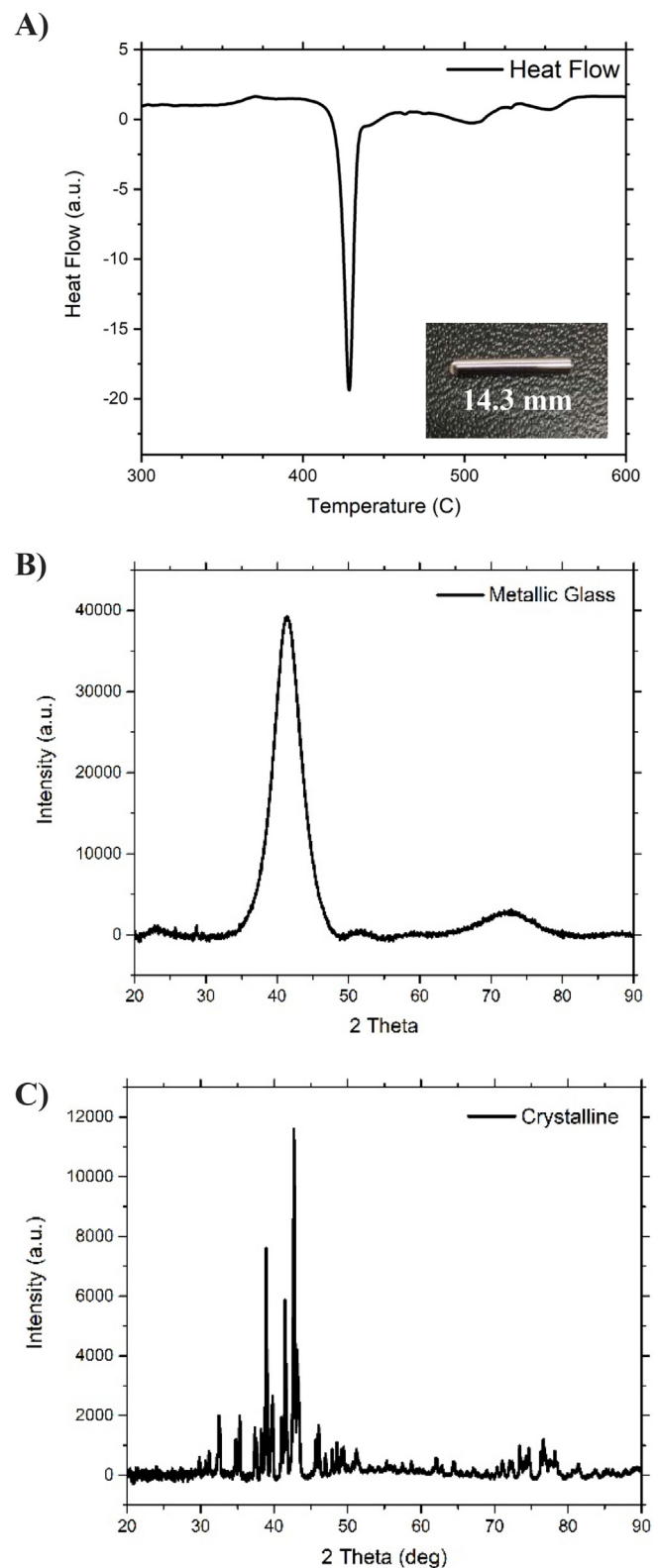

Fig. 1. A) Differential scanning calorimetry (DSC) thermogram indicating glass transition and crystallization temperature of an as-cast amorphous Pd77.5Cu6Si16.5, inset of as-cast rod. **B)** X-Ray diffraction characterization of amorphous and **C)** crystalline sample showing intense peaks.

plane of incidence. R_P and R_S represent the complex Fresnel coefficients for p and s-polarizations, respectively. This ratio is defined as shown in (1)

$$\rho = \frac{R_p}{R_s} = \tan(\psi)e^{i\Delta} \qquad (1)$$

Details of the VASE technique are discussed elsewhere [32–36]. Briefly, this technique requires data analysis based on an optical model corresponding to the structure of the sample. Optical modeling and data analysis were done using the Woollam Company CompleteEASE software package. With the bulk sample conditions satisfied, we could relate Ψ and Δ directly to the optical constants n and k by the complex refractive index as shown in (2) where ρ is the ratio from (1).

$$\tilde{n}^2 = \sin^2(\phi) * \left[1 + \tan^2(\phi) * \left(\frac{1-\rho}{1+\rho} \right)^2 \right] \qquad (2)$$

This exact equation, however, would include noise in the optical constants and cannot guarantee Kramers-Kronig consistency. For this reason, multiple angles and wavelengths were fit simultaneously in the optical models using b-spline method constrained (by CompleteEASE software) to obey Kramers-Kronig relations. This b-spline fitting allows flexible shape for the optical properties while maintaining smooth, continuous and physical curves with minimum number of fit parameters. We measured ten distinct locations on each sample, and we illustrate the averaged optical constants for the specimen after fit and compare these values to the published optical data of pure Pd [37] (Fig. 2). We observe that both n and k are featureless and increase monotonically across the range of measured wavelengths.

3. Results and discussion

The refractive index is greater than 1 for nearly all measured wavelengths (Fig. 2(a)). We observed that pure crystalline Pd is also monotonically increasing however its refractive index falls below the crystalline alloy, and greater than the metallic glass alloy. It is evident that light travels faster in the metallic glass alloy relative to the pure crystalline Pd sample, but light travels slower in the crystalline alloy than the pure crystalline Pd sample. The presence of Cu and Si increase the occurrence of defects in the crystal lattice thereby contributing to the reduced speed of light at all frequencies. The crystalline alloy sample exhibits higher values of both n and k, which likely stem from higher mass density and translational periodicity when compared to the homogeneous metallic glass sample. As Pena-Rodriguez et al. determined, and we also observe here, the refractive index of an alloy is not predictable by a combination of its constituent elements [38]. The refractive index data was used to generate the dielectric function reported in Fig. S3.

The refractive index data can also be used to calculate the conduction band energy of the bulk specimens [39]. It is a convenient way of studying the optical absorption spectrum of a material. The absorption coefficient α can be calculated from the extinction coefficient k by (3).

$$\alpha = (4\pi k)/\lambda \qquad (3)$$

In order to calculate the conduction band energy of $Pd_{77.5}Cu_6Si_{16.5}$ alloy we use the Tauc relationship as follows [39] in (4) where $h\nu$ is the photon energy, E_{cb} is the conduction band energy, and B is constant.

$$(\alpha h\nu)^2 = B(h\nu - E_{cb}) \qquad (4)$$

We compute the absorption coefficient in the range of 300–2000 nm according to Equation (3) and fit Equation (4) to the calculated data. The calculated data (symbols) and fitted curve are shown in Fig. 3. By extrapolating the linear portion of the plot versus photon energy $h\nu$ to $(\alpha h\nu)^2 = 0$, the conduction band energy can be found as shown in Fig. 3. Various regions were used for linear fits and averaged to determine the conduction band energy and resulting uncertainty (Figs. S1 and S2). For all linear fits used, the Pearson's R^2 was greater than 0.99 for all fits. The resulting Tauc plots in Fig. 3 of the metallic glass sample, in which the fitted line reveals a conduction band energy of
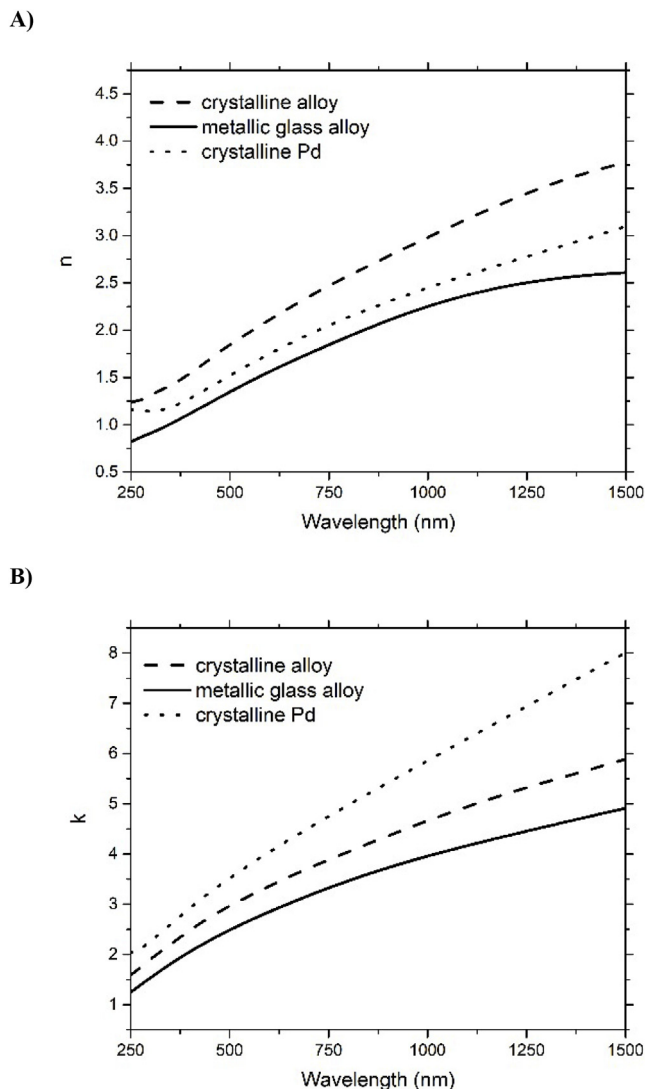
A)

B)

Fig. 2. Optical constants **A)** refractive index and **B)** extinction coefficient for crystalline and metallic glass alloys, and pure Pd [39].
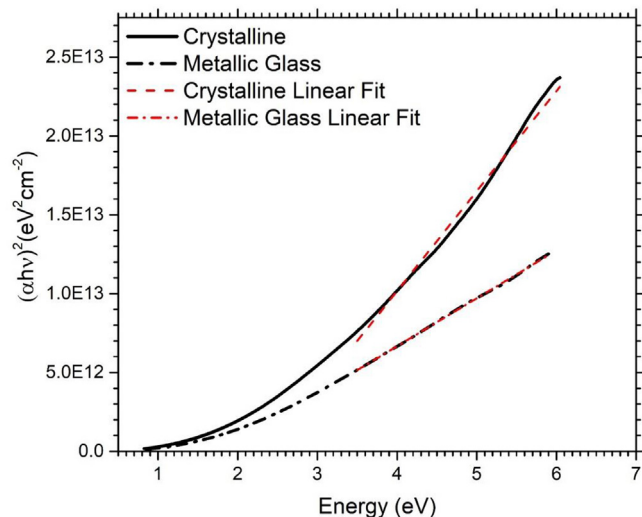
Fig. 3. Tauc plot computing the conduction band energy of bulk metallic glass and crystalline alloy.

1.78 ± 0.06 eV and the crystalline sample band energy of 2.32 ± 0.03 eV. The various linear regions and fit parameters can be found in Tables S1 and S2. We observe that the conduction band energy increases in the crystalline sample when compared to the metallic glass.

It is expected that the crystalline sample would have a different conduction band energy than the metallic glass as Brillouin zone boundary changes due to symmetry breaking in the amorphous (metallic glass) material. The crystalline sample has a lattice periodicity with translational symmetry that will not be present in the amorphous sample and conduction band energy is strongly tied to the periodicity of a lattice. In the crystalline sample, long-range order causes sharp Brillouin zone boundaries in k-space. The electron states, satisfying Bloch's theorem, in the crystalline sample can be described as Bloch waves extending throughout the crystal. Whereas in the metallic glass sample, there is no long-range order, a unit cell no longer exists, there is no k-space, and consequently, Bloch's theorem is inapplicable [40]. Despite the loss of long-range order in the metallic glass sample, short-range order is still present, causing diffraction halos corresponding to pseudo-Brillouin zones with blurred boundaries [41,42]. Since the band energy is strongly tied to the degree of periodicity of the lattice, the Brillouin zone boundary differences between these materials result in distinct conduction band energy levels. Additionally, we characterized the magneto-electrical transport response in the Van der Pauw configuration. The Hall measurements were conducted with a Bio-Rad HL 5500 Hall system. As disorder has a strong influence on electronic transport, the crystalline sample exhibits lower sheet resistance (25 ± 2.40 vs. $39 \pm 3.64\,\Omega/sq$) and lower mobility (0.6 ± 0.115 vs. 1.9 ± 0.088 cm^2/V-s), from which we infer that the crystalline material has more electrically active defect sites than the amorphous material (Table S3).

It is well known that the optical and electronic characterization of novel materials is arduous [38]. There is growing interest in implementing machine learning and neural networks to expedite this cumbersome process [43,44]. Through the investigation of the conduction band energy here we uncover a discriminator that could be further considered for implementation for utility in modeling these systems. The conduction band is a distinct value that is obtained optically and provides a means of classifying the crystalline structure of the Pd77.5Cu6Si16.5 alloy. This could enable a decision tree classifier where one could simply measure or extract the optical properties of this alloy to determine the structure of the material essentially bypassing x-ray diffraction measurements traditionally used for this purpose. We propose this characterization can be further explored and tuned as this alloy is further characterized at various degrees of crystallinity and other discrete values are isolated to further inform a model.

Here we present the first measured optical constants of amorphous and crystallized $Pd_{77.5}Cu_6Si_{16.5}$ alloy. This alloy is among the most highly studied BMGs, mainly due to its high glass forming ability [25] as it can be co-sputtered as a thin film [29] and fabricated in bulk reaching critical size greater than 1 cm [26]. BMGs possess an excellent combination of properties, such as high values of yield strength, elasticity, corrosion resistance, polymer-like thermoplastic formability, and excellent magnetic properties, rendering this class of materials highly suitable for myriad applications. BMGs have already been implemented in numerous technological applications including catalysis, micro and macro devices (i.e. fuel cells, microcantilevers, electrical current sensors) and biomedical devices [45]. Despite the recent vast exploration of BMGs, considerations for optical integration have lagged. BMGs are suitable for application as optical mirrors of various shapes and as connecting parts in optical fibers [46]. By presenting the measured optical constants of the versatile $Pd_{77.5}Cu_6Si_{16.5}$ alloy, here we aim to motivate researchers in optical application spaces to consider this formable metallic glass, and the greater class of BMG materials, for optical device applications.

4. Conclusion

In this study, amorphous and crystallized $Pd_{77.5}Cu_6Si_{16.5}$ bulk samples have been optically characterized. The optical properties of this alloy have been investigated by X-ray diffraction, spectral ellipsometry, and conduction band energy calculations. We observe monotonically increasing refractive indices for the metallic glass alloy, pure crystalline Pd, and crystalline alloy, respectively. We demonstrate by Tauc plot analysis that the conduction band energy increases from 1.78 ± 0.06 eV in the amorphous material to 2.32 ± 0.03 eV in the bulk crystalline specimen. Here we motivate the use of these distinct optical properties as a means to enable decision tree modeling for machine learning applications in materials classification, design, and implementation. These findings may be useful towards optimizing the performance of $Pd_{77.5}Cu_6Si_{16.5}$ for an array of optical device applications.

Notes

The authors declare no competing financial interests.

Declaration of interests

The authors declare that they have no known competing financial interests or personal relationships that could have appeared to influence the work reported in this paper.

Author contributions

The manuscript was written through contributions of all authors. All authors have given approval to the final version of the manuscript.

Acknowledgments

Appendix A. Supplementary data

Supplementary data to this article can be found online at https://doi.org/10.1016/j.omx.2019.100012.

Funding sources

References

[1] W. Klement, R. Willens, P. Duwez, Nature 187 (1960) 869–870.
[2] J. Schroers, Adv. Mater. 22 (2010) 1566–1597.
[3] J. Schroers, B. Lohwongwatana, W.L. Johnson, A. Peker, Appl. Phys. Lett. 87 (2005) 061912Art. No..
[4] J. Schroers, W.L. Johnson, Phys. Rev. Lett. 93 (2004) 255506.
[5] A. Inoue, B. Shen, H. Koshiba, H. Kato, A.R. Yavari, Nat. Mater. 2 (2003) 661–663.

[6] M. Ashby, A. Greer, Scripta Mater. 54 (2006) 321–326.
[7] M. Carmo, R.C. Sekol, S.Y. Ding, G. Kumar, J. Schroers, A.D. Taylor, ACS Nano 5 (2011) 2979–2983.
[8] S. Mukherjee, M. Carmo, G. Kumar, R.C. Sekol, A.D. Taylor, J. Schroers, Electrochim. Acta 74 (2012) 145–150.
[9] S. Mukherjee, R.C. Sekol, M. Carmo, E.I. Altman, A.D. Taylor, J. Schroers, Advanced Functional Materials, (2013) (n/a-n/a).
[10] R.C. Sekol, G. Kumar, M. Carmo, F. Gittleson, N. Hardesty-Dyck, S. Mukherjee, J. Schroers, A.D. Taylor, Small 9 (2013) 2081–2085.
[11] G. Doubek, R.C. Sekol, J. Li, W.H. Ryu, F.S. Gittleson, S. Nejati, E. Moy, C. Reid, M. Carmo, M. Linardi, Adv. Mater. 28 (2016) 1940–1949.
[12] J.-W. Jung, W.-H. Ryu, J. Shin, K. Park, I.-D. Kim, ACS Nano 9 (2015) 6717–6727.
[13] H.J. Tarigan, N. Kahler, N.S. Ramos, G. Kumar, A.A. Bernussi, Appl. Phys. Lett. 107 (2015) 021903.
[14] J.P. Singer, M. Gopinadhan, Z. Shao, A.D. Taylor, J. Schroers, C.O. Osuji, ACS Appl. Mater. Interfaces 7 (2015) 3456–3461.
[15] J. Li, F.S. Gittleson, Y. Liu, J. Liu, A.M. Loye, L. McMillon-Brown, T.R. Kyriakides, J. Schroers, A.D. Taylor, Chem. Commun. 53 (2017) 8288–8291.
[16] A. Masood, T. Tamaki, V. Ström, A. Borgenstam, J. Ågren, K.V. Rao, IEEE Trans. Magn. 50 (2014) 4004005.
[17] S. Tanaka, T. Kaneko, N. Asao, Y. Yamamoto, M. Chen, W. Zhang, A. Inoue, Chem. Commun. 47 (2011) 5985–5987.
[18] M. Carmo, R.C. Sekol, S. Ding, G. Kumar, J. Schroers, A.D. Taylor, ACS Nano 5 (2011) 2979–2983.
[19] E.R. Kinser, J. Padmanabhan, R. Yu, S.L. Corona, J. Li, S. Vaddiraju, A. Legassey, A. Loye, J. Balestrini, D.A. Solly, ACS Sens. 2 (2017) 1779–1787.
[20] M. Kanik, P. Bordeenithikasem, G. Kumar, E. Kinser, J. Schroers, Appl. Phys. Lett. 105 (2014) 131911.
[21] M. Kanik, P. Bordeenithikasem, D. Kim, N. Selden, A. Desai, R. M'Closkey, J. Schroers, J. Microelectromech. Syst. 24 (2015) 19–28.
[22] G. Kumar, P.A. Staffier, J. Blawzdziewicz, U.D. Schwarz, J. Schroers, Appl. Phys. Lett. 97 (2010).
[23] E. Garnett, P. Yang, Nano Lett. 10 (2010) 1082–1087.
[24] H.A. Atwater, A. Polman, Nat. Mater. 9 (2010) 205–213.
[25] H. Chen, D. Turnbull, Acta Metall. 17 (1969) 1021–1031.
[26] D. Hong-Yu, L. Yang, Y. Ke-Fu, Chin. Phys. Lett. 27 (2010) 126101.
[27] A. Schlegel, P. Wachter, K. Ackermann, M. Liard, H.-J. Güntherodt, Solid State Commun. 31 (1979) 373–376.
[28] R. Lapka, G. Leemann, H.-J. Güntherodt, Mater. Sci. Eng. 99 (1988) 313–316.
[29] Y. Liu, S. Hata, K. Wada, A. Shimokohbe, Jpn. J. Appl. Phys. 40 (2001) 5382.
[30] H.W. Kui, A.L. Greer, D. Turnbull, Appl. Phys. Lett. 45 (1984) 615–616.
[31] J. Schroers, Y. Wu, W.L. Johnson, Philos. Mag. A 82 (2002) 1207–1217.
[32] J.A. Woollam, P.G. Snyder, Mater. Sci. Eng., B 5 (1990) 279–283.
[33] S.A. Alterovitz, J.A. Woollam, P.G. Snyder, Solid State Technol. 31 (1988) 99–102.
[34] J.N. Hilfiker, N. Singh, T. Tiwald, D. Convey, S.M. Smith, J.H. Baker, H.G. Tompkins, Thin Solid Films 516 (2008) 7979–7989.
[35] J.A. Woollam, B.D. Johs, C.M. Herzinger, J.N. Hilfiker, R.A. Synowicki, C.L. Bungay, Overview of Variable-Angle Spectroscopic Ellipsometry (VASE): I. Basic Theory and Typical Applications, Optical Metrology: A Critical Review, International Society for Optics and Photonics, 1999, p. 1029402.
[36] B. Johs, J.A. Woollam, C.M. Herzinger, J.N. Hilfiker, R.A. Synowicki, C.L. Bungay, Overview of Variable-Angle Spectroscopic Ellipsometry (VASE): II. Advanced Applications, Optical Metrology: A Critical Review, International Society for Optics and Photonics, 1999, p. 1029404.
[37] P.B. Johnson, R.W. Christy, Phys. Rev. B 9 (1974) 5056–5070.
[38] O. Peña-Rodríguez, M. Caro, A. Rivera, J. Olivares, J.M. Perlado, A. Caro, Opt. Mater. Express 4 (2014) 403–410.
[39] L. Gharibshahi, E. Saion, E. Gharibshahi, A.H. Shaari, K.A. Matori, Materials 10 (2017) 402.
[40] P. Häussler, Phys. Rep. 222 (1992) 65–143.
[41] G.S. Grest, S.R. Nagel, A. Rahman, Phys. Rev. Lett. 49 (1982) 1271–1274.
[42] J. Hafner, J. Non-Cryst. Solids 75 (1985) 253–258.
[43] G. Pilania, C. Wang, X. Jiang, S. Rajasekaran, R. Ramprasad, Sci. Rep. 3 (2013) 2810.
[44] K. Schütt, H. Glawe, F. Brockherde, A. Sanna, K. Müller, E. Gross, Phys. Rev. B 89 (2014) 205118.
[45] M.M. Khan, A. Nemati, Z.U. Rahman, U.H. Shah, H. Asgar, W. Haider, Crit. Rev. Solid State Mater. Sci. 43 (2018) 233–268.
[46] A. Inoue, X. Wang, W. Zhang, Rev. Adv. Mater. Sci. 18 (2008) 1–9.